Report

Current Biology

Nanoscale Visualization of Biomineral Formation in Coral Proto-Polyps

Highlights

- Coral biomineral formation begins as intracellular pockets of concentrated calcium
- This calcium concentration is mediated by highly acidic (Asp-rich) proteins
- Ca^{2+} and proteins are exported and aragonite nucleation commences extracellularly
- Crystals elongate outward from extracellular matrix proteins on the cells' surface

Authors

Tali Mass, Jeana L. Drake, John M. Heddleston, Paul G. Falkowski

Correspondence

tmass@univ.haifa.ac.il

In Brief

Using coral cell cultures, Mass et al. show that the stony coral biomineralization mechanism begins with intracellularly concentrated calcium, which is exported for extracellular crystal nucleation and growth. Aragonite crystals elongate outward from an extracellular protein matrix into the culture medium.

Mass et al., 2017, Current Biology *27*, 3191–3196
October 23, 2017
https://doi.org/10.1016/j.cub.2017.09.012

CellPress

Current Biology
Report

Nanoscale Visualization of Biomineral Formation in Coral Proto-Polyps

Tali Mass,[1,6,7,*] Jeana L. Drake,[2,5,6] John M. Heddleston,[3] and Paul G. Falkowski[2,4]
[1]University of Haifa, Department of Marine Biology, The Leon H. Charney School of Marine Sciences, Multi Purpose Boulevard, Mt. Carmel, Haifa 3498838, Israel
[2]Rutgers University, Department of Marine and Coastal Sciences, Dudley Road, New Brunswick, NJ 08901, USA
[3]Howard Hughes Medical Institute Janelia Research Campus, Advanced Imaging Center, Helix Drive, Ashburn, VA 20147, USA
[4]Rutgers University, Department of Earth and Planetary Sciences, Taylor Road, Piscataway, NJ 08854, USA
[5]Present address: Department of Ecology and Evolutionary Biology, University of California, Los Angeles, Charles E. Young Drive, Los Angeles, CA 90095, USA
[6]These authors contributed equally to this work
[7]Lead Contact
*Correspondence: tmass@univ.haifa.ac.il
https://doi.org/10.1016/j.cub.2017.09.012

SUMMARY

Calcium carbonate platforms produced by reef-building stony corals over geologic time are pervasive features around the world [1]; however, the mechanism by which these organisms produce the mineral is poorly understood (see review by [2]). It is generally assumed that stony corals precipitate calcium carbonate extracellularly as aragonite in a calcifying medium between the calicoblastic ectoderm and pre-existing skeleton, separated from the overlying seawater [2]. The calicoblastic ectoderm produces extracellular matrix (ECM) proteins, secreted to the calcifying medium [3–6], which appear to provide the nucleation, alteration, elongation, and inhibition mechanisms of the biomineral [7] and remain occluded and preserved in the skeleton [8–10]. Here we show in cell cultures of the stony coral *Stylophora pistillata* that calcium is concentrated in intracellular pockets that are subsequently exported from the cell where a nucleation process leads to the formation of extracellular aragonite crystals. Analysis of the growing crystals by lattice light-sheet microscopy suggests that the crystals elongate from the cells' surfaces outward.

RESULTS AND DISCUSSION

Over the past decades, biomineralization mechanisms have been extensively investigated in various metazoans, leading to several broad hypotheses [11, 12]. One relates to the extracellular involvement of specific highly acidic extracellular matrix (ECM) proteins (containing > 30% aspartic [Asp] and glutamic [Glu] acids) that have specific roles in mineral nucleation, growth, modification, and inhibition [13, 14]. For stony corals, there is evidence that a family of coral acid-rich proteins (CARPs) employs the carboxyl groups of the two acidic amino acids to coordinate free Ca^{2+} ions *in vitro*, thereby initiating a Lewis acid reaction that displaces a proton on bicarbonate anions, leading to the precipitation of carbonate on the trapped calcium atoms [7]. This reaction ultimately leads to the formation of aragonite crystals [7]. Another hypothesis proposes that ACC precursor nanoparticles are deposited in microenvironments that are enriched in skeletal organic matrix (SOM) secreted by the animal [15, 16]. There is compelling evidence for this process in zebrafish bone [17], chicken embryo bone [18], sea urchins [19], and foraminifera [20], but an analogous phenomenon has yet to be shown conclusively in corals. The two hypotheses are not mutually exclusive. Here, we combine immuno-labeling, lattice light-sheet microscopy (LLSM), and nano-scale secondary ion mass spectrometry (NanoSIMS) to generate high-resolution images across all four dimensions of space-time simultaneously in proto-polyps derived from coral cell cultures. We show that the biomineralization process is initiated intracellularly by highly acidic proteins that aggregate calcium, which is transported to the cell surface. There, additional acidic proteins nucleate and elongate new aragonite crystals extracellularly.

Coral cell cultures that contain all cell types, while not maturing to adult polyps, are useful model systems to study biomineralization. We have previously shown that within ~72 hr after isolation, cultures of separated coral cells aggregate into proto-polyps and form extracellular crystals of aragonite [21, 22] at a rate comparable to the intact organism and with geochemical properties similar to parent skeleton [23]. Confocal microscopy of immuno-labeled proto-polyps of the Indo-Pacific stony coral *Stylophora pistillata* showed that two CARP proteins (CARPs 1 and 4; Figure 1A and Figures S1 and S2, respectively) were secreted and preferentially localized to the ECM surrounding coral cells. This ECM has previously been shown to adhere proto-polyp cells to each other [21]. Concomitantly, LLSM images revealed that the calcein label is observed in the ECM, suggesting that calcium ions are initially recruited by these proteins on the ECM covering the surface of the proto-polyps in a way that remains unclear (Figure 2, Movie S1). It should be noted that intense calcein fluorescence on the surface of the proto-polyps was at interfaces

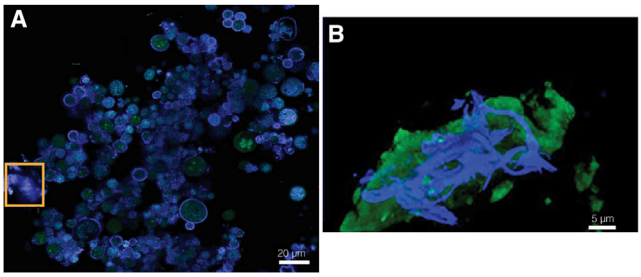

Figure 1. Imaging CARP1 and Calcein in Proto-Polyps and Crystals

(A) Confocal microscope image of fluorescently labeled CARP1 antibodies (blue) immunolocalized to extracellular matrix (ECM) proteins on the surface of coral proto-polyps cells on day 5. The light blue spheres are the individual cells of the proto-polyp, which are attached to each other by ECM [21, 22], here immuno-labeled for CARP1.

(B) Higher magnification of the region depicted in the orange box in (A) shows a newly forming $CaCO_3$ crystal labeled with calcein (green) that is attached to immuno-labeled CARP1in the ECM (blue). (B) is a composite of the same crystal imaged by confocal microscopy for CARP1 immunolocalization and two-photon microscopy for calcein labeling.

Scale bars: (A), 20 μm; (B), 5 μm. See also Figures S1 and S2.

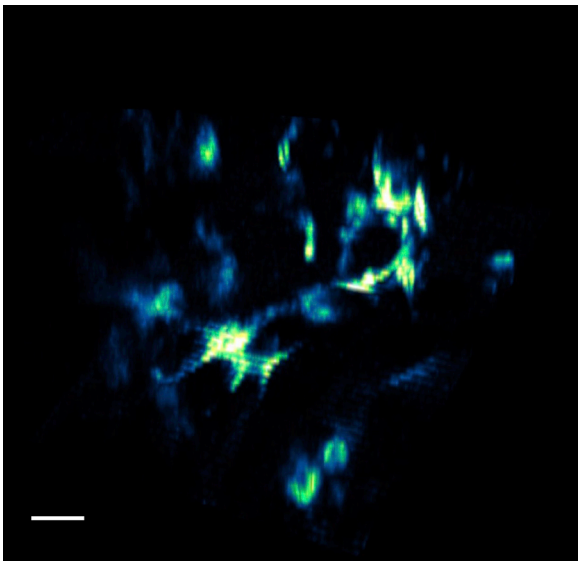

Figure 2. Imaging Calcein in Proto-Polyp ECM

Lattice light-sheet microscopy (LLSM) image of calcein incorporated into the ECM on the surface of proto-polyp cells on days 2–3. The LLSM's 300 mW MPB laser (488 nm) captures only the fluorescence signal of calcein. Minor background fluorescence from the calcein in the media caused a negative imaging affect for the cells; therefore, cells appear as round black shapes within the green calcein attached to the ECM. Color intensity is due to the z axis of the cells and is not indicative of calcein concentration. Scale bar, 10 μm. See also Movie S1.

between the cells' surfaces and the nutrient-amended seawater medium. Additionally, CARP1 was specifically localized not only within ECM proteins, but also adjacent to newly formed crystals (Figure 1B).

Time series of LLSM images allowed us to observe the incorporation of calcein into individual crystals as they grew on the surface of living proto-polyps (Figure 3A, Movie S2). Crystals of ~2 μm width grew outward from the ECM on the surface of the cells into the growth medium. At ambient temperature of 25°C, the crystals extended at a rate of 0.07 ± 0.03 μm min^{-1}. Similar-sized crystals, observed by scanning electron microscopy (SEM) on proto-polyps, confirmed that crystals were indeed embedded within the ECM (Figure 3B). Energy-dispersive X-ray spectroscopy (EDS) analysis indicated that, in addition to Ca, these nascent crystals contained Mg (Figure 3C).

Based on the extension rate of the calcein incorporation, we calculated growth rates for ten separate crystals within a single culture (Table S1). Previous work has shown that *S. pistillata* cell cultures precipitate aragonite [21]. Using an aragonite density of 2.93 g cm^{-3} [24], we calculated growth rates of single crystals from 0.10 fg to 1.36 pg $CaCO_3$ hr^{-1}. For comparison, individual crystals of aragonite bundles produced by mollusk pearl sac cultures appear to grow at an overall rate on the order of 1 pg $CaCO_3$ $hr^{-1,}$ [25]. In contrast, coral cell cultures precipitate $CaCO_3$ at a culture-wide rate on the order of 1,000–10,000 pg (μg $protein^{-1}$) hr^{-1} [23], which is similar to that calculated for growth rates of intact coral nubbins [26]. While we observed a very large range in growth rates (Table S1), the average rate calculated from single crystals appears to be indicative of the ensemble rate in intact corals.

After 12-day growth of *S. pistillata* proto-polyps, we co-located areas of Asp-based $\delta^{15}N$ enrichment (as $^{12}C^{15}N^-/^{12}C^{14}N^-$), associated with highly acidic proteins, with ^{40}Ca using NanoSIMS (Figure 4A). Like immunolocalized CARPs 1 and 4 (Figures 1 and S1B, respectively), the enriched $\delta^{15}N$ signal was often more concentrated at the edges of cells. Multiple regions of multi-pixel ^{15}N enrichment were observed, notably in the same pixel as or adjacent to $^{40}Ca^-$. Where enriched $\delta^{15}N$ co-localized to the same pixel as $^{40}Ca^-$, the isotopic enrichment averaged 0.0077‰ (SD 0.0027‰), suggesting that highly acidic proteins incorporating the labeled Asp were in contact with the concentrated calcium. Post-SIMS EDS spot analysis of regions of interest (ROIs) supports the detection of intracellular and membrane-associated $^{40}Ca^-$ concentration by NanoSIMS (Figures 4B and 4C). It also reveals that that these regions contained Na and Mg. The mineral composition of these intracellular Ca aggregations remains to be determined.

The combination of biochemical and imaging tools used here strongly suggests that $CaCO_3$ biomineralization in coral proto-polyps is initiated intracellularly in areas that contain Asp-rich proteins similar to or including CARPs. The areas containing the concentrated calcium are exported to the cell surface, where they are evaginated or secreted, and the biomineral matures as extracellular crystals. These observations explain previous work showing that the biomineralization process does not *require* a calicoblastic space for the formation of aragonite [21]; the process commences intracellularly with calcium concentration and proceeds to membrane-bound and extracellular locations for crystal nucleation and growth. The extracellular process of crystal growth is likely aided by proteins such as Ca-ATPases and carbonic anhydrases that further concentrate Ca and provide sufficient HCO_3^- within the calicoblastic space [27, 28].

To the best of our knowledge, this is the first-time LLSM and SIMS have been used to observe this process in corals, but it has analogs in other calcifying marine protists and invertebrates.

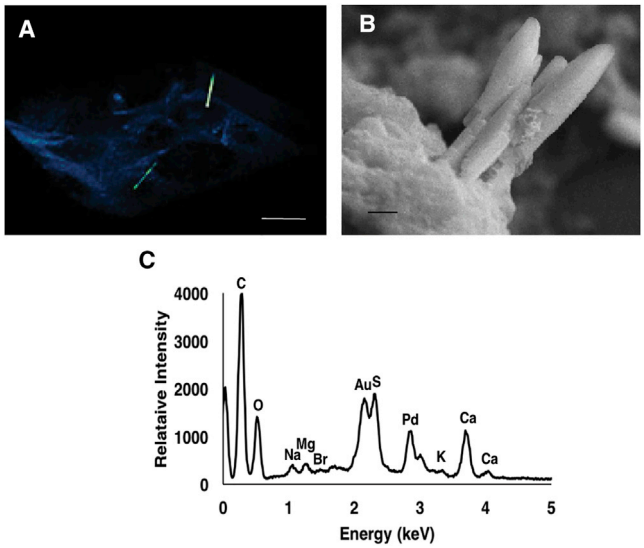

Figure 3. Proto-Polyp Crystal Growth and Elemental Content

(A) Growth of calcium-bearing crystals outward from the extracellular organic matrix on days 4–5 as indicated by calcein incorporation into newly formed crystals, here appearing as thin needle shapes. The blue signal in the image is part of the look-up table and made to emphasize the low end of the histogram. It was enhanced post-processing in order to show the cells in "negative relief" since the cell body would not take up calcein.

(B) SEM of the edge of a 9-day-old proto-polyp in which similarly sized extracellular aragonite crystals were observed.

(C) EDS of crystals shown in (B); Au and Pd peaks are from the gold coating. Scale bars: (A), 10 μm; (B), 2 μm. See also Table S1 and Movie S2.

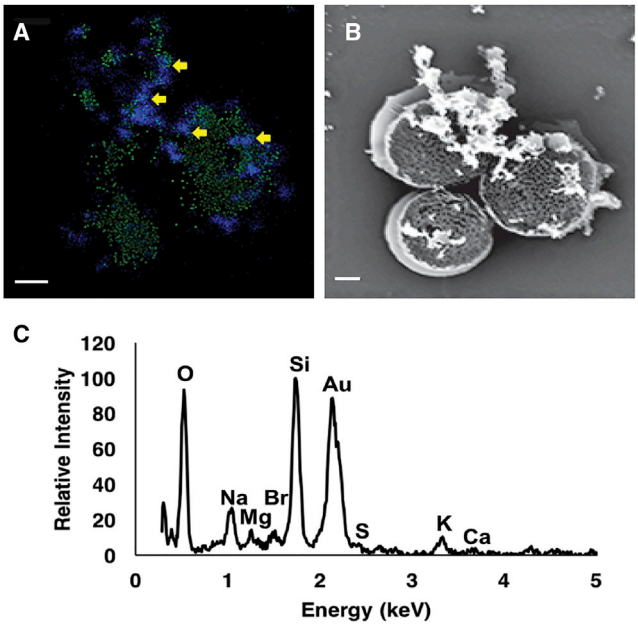

Figure 4. NanoSIMS δ^{15}N and $^{40}Ca^-$ Co-localization

(A–C) NanoSIMS (A) co-localization of δ^{15}N enrichment > 0.0036 ‰ (green) and $^{40}Ca^-$ (blue) as indicated by the yellow arrows, (B) post-SIMS electron micrograph of the proto-polyp with $CaCO_3$ nanoparticles, and (C) EDS spectrum of nanoparticles. The Au and Si peaks are from the gold coating and the silica wafer substrate, respectively. Scale bar, 1 μm. See also Table S2.

Initial aggregation of calcium carbonate in intracellular vesicles has been suggested in foraminifera, mollusks, coralline demosponges, and sea urchins, generally beginning as amorphous calcium carbonate (ACC) [19, 20, 29–31]. Although vesicles containing high concentrations of intracellular calcium have been reported previously, both membrane-bound and within the cytosol in the stony coral *Pocillopora damicornis* [32, 33], the observations were subsequently suggested to be artifacts of sample preparation [34]. Moreover, only extracellular spherical structures that resemble these vesicles were observed in carefully prepared Pocilloporid coral samples [35]. Our results, based on NanoSIMS and SEM-EDS data, strongly support an intracellular calcium concentration process. Our immunolocalization results further suggest that CARPs mediate the process of initial calcium carbonate formation as it proceeds from an intra- to extracellular locations.

Although NanoSIMS analyses reveal Asp-associated ^{15}N signals throughout *S. pistillata* cells, we observed the highest concentrations at cell membranes as well as multiple locations of its co-localization with Ca aggregations. Labeled amino acid incubations were within time constraints previously shown to result in both minimal conversion of Asp to other residues and incorporation into coral biomineralization proteins [36], so we are confident that these enriched δ^{15}N signals are indeed representative of concentrated Asp in proteins such as CARPs. CARP4 was predicted in all three queried servers to contain transmembrane regions for anchorage to the cell membrane (Table S2), supporting membrane-associated ^{15}N enrichment. Additionally, CARP4 has been specifically immunolocalized to the membranes of desmocytes in intact corals [3]. Assuming complete ^{15}N-Asp enrichment of CARP4, an approximately 40 kDa protein, it is quite possible that the pixilation of enrichment at cell edges is due to nugget effects of a single highly enriched CARP4 molecule per pixel among other minimally labeled (i.e., not high Asp-containing) transmembrane proteins.

Intracellularly, CARP4 and other CARPs likely perform the first step of concentrating calcium. As the process continues to extracellular locations, the carboxyl-rich CARPs could serve to prevent mineral nucleation by increasing the energy barrier to nucleation [37, 38]. CARPs could also stabilize ACC or other unstable phases [39] similar to the roles of Asprich or Pfn44. Both of these acidic molluscan proteins have been shown to stabilize ACC and high-Mg calcite [40, 41]. Using SEM-EDS, we detected Mg co-localizing with Ca in extracellular crystals and spherical intracellular aggregates (Figures 3C and 4C, respectively). High concentrations of Mg were previously reported at corals' centers of calcification [15, 42], and a recent study suggests that magnesium-rich ACC initiates the biomineralization process [15]. X-ray diffraction work on *S. pistillata* cell cultures by Mass et al. [21] includes a Mg-calcite peak at ~30 2θ in addition to the XRD peaks characteristic of aragonite, which the authors did not note at the time. Calcein binds 2^+ ions including both Ca and Mg; hence our LLSM tracking of ECM and $CaCO_3$ production may also indicate Mg incorporation [20]. The proposed mechanism for mineral initiation in corals would allow for Mg-calcite, as it suggests that highly acidic proteins such as CARPs coordinate calcium ions

with 2^+ charge [7] that could be replaced by Mg^{2+}. A transient or small amount of Mg-calcite at the site of initial $CaCO_3$ precipitation may also explain the presence of Mg observed in centers of calcification in parent skeleton [42].

Following transport of mineral precursor components to extracellular sites of nucleation, it appears that CARPs and Mg are potentially involved in the subsequent formation of aragonite [15]. Confocal imaging showed CARPs1 and 4 immunolocalized to discrete positions within the ECM surrounding cells while LLSM indicates that this ECM extensively binds Ca^{2+} ions. Additionally, LLSM and confocal microscopy revealed that CARP1 is localized to calcein-binding crystals. Several CARPs have previously been immunolocalized to various tissue layers and components of coral skeleton; most notably, CARPs 1 and 4 are found in early mineralization zones of adult skeleton, suggesting that they play a role in aragonite nucleation [3].

Based on our findings, we propose the following process for initial $CaCO_3$ precipitation by coral cells. Intracellular regions, possibly of vesicular origin, high in Asp- or Glu-content proteins such as CARPs, transport Ca^{2+} ions to the surface of the cells and might be further concentrated in centers of calcification of intact coral polyps. The mineral precursor, which remains to be distinguished, is formed extracellularly and subsequently interacts with other ECM proteins to be converted to aragonite as the proto-polyp grows. In the proto-polyp model we used here, aragonite crystals grow outward from the ECM into the overlying growth medium in a particle attachment process similar to the one described for other systems [11].

Our results suggest that the biomineralization process in corals, while ultimately proceeding to aragonite extracellularly, begins intracellularly far from chemical equilibrium. The commencement of the biomineralization process does not require a calcioblastic space, and the growth rates of single crystals observed in coral cell cultures are comparable both to intact coral nubbins and to other biomineralizing invertebrates.

STAR★METHODS

Detailed methods are provided in the online version of this paper and include the following:

- KEY RESOURCES TABLE
- CONTACT FOR REAGENT AND RESOURCE SHARING
- EXPERIMENTAL MODEL AND SUBJECT DETAILS
- METHOD DETAILS
  - Cell culture preparation
  - Antibody staining
  - Lattice light sheet microscopy (LLSM) sample preparation
  - ^{15}N Labeling and Secondary Ion Mass Spectrometry (SIMS)
  - CARPs Transmembrane Prediction
- QUANTIFICATION AND STATISTICAL ANALYSIS
  - Antibody Staining
  - LLSM Calcein Imaging
  - ^{15}N Labeling and Secondary Ion Mass Spectrometry (SIMS)
- DATA AND SOFTWARE AVAILABILITY
  - LLSM Single Crystal Growth Rate

SUPPLEMENTAL INFORMATION

Supplemental Information includes two figures, two tables, and two movie and can be found with this article online at https://doi.org/10.1016/j.cub.2017.09.012.

AUTHOR CONTRIBUTIONS

Conceptualization, T.M., J.L.D., J.H., P.G.F.; Investigation, T.M., J.L.D.; Formal Analysis, T.M., J.L.D., J.H.; Data Curation, T.M.; Writing – Original Draft, T.M., J.L.D. with input from J.H. and P.G.F.; Writing – Review & Editing, T.M., J.L.D., J.H., P.G.F.; Visualization, T.M., J.L.D.; Funding Acquisition, T.M., J.L.D., P.G.F.

ACKNOWLEDGMENTS

We thank J. Yaiullo of the Long Island Aquarium and Exhibition Center for coral nubbins, J. Adkins and Y. Guan at the CalTech Microanalysis Center for comments and technical assistance, and M. Pierce and N. Tumer at the Rutgers SEBS Core Facility Imaging Center. Additional imaging data used in this publication were produced in collaboration with the Advanced Imaging Center, a facility jointly supported by the Gordon and Betty Moore Foundation and the Howard Hughes Medical Institute. We thank V. Starovoytov, A. Fu, and M. Stern for technical assistance; E. Sweid for code assistance; and the Thor lab at the two-photon facility. We also thank three anonymous reviewers for insightful comments. The authors acknowledge funding from the National Science Foundation (Award EF-1416785) to P.G.F. and T.M.; Israel Science Foundation (Grant 312/15) to T.M.; and Sigma Xi GIAR (Award 280801) to J.L.D.

Received: May 18, 2017
Revised: July 11, 2017
Accepted: September 6, 2017
Published: October 12, 2017

REFERENCES

1. Spalding, M.D., Green, E.P., and Ravilious, C. (2001). World Atlas of Coral Reefs (Berkeley: University of California Press).
2. Allemand, D., Tambutté, É., Zoccola, D., and Tambutté, S., eds. (2011). Coral calcification, cells to reefs, *Volume 3* (New York: Springer).
3. Mass, T., Drake, J.L., Peters, E.C., Jiang, W., and Falkowski, P.G. (2014). Immunolocalization of skeletal matrix proteins in tissue and mineral of the coral Stylophora pistillata. Proc. Natl. Acad. Sci. USA *111*, 12728–12733.
4. Mass, T., Putnam, H.M., Drake, J.L., Zelzion, E., Gates, R.D., Bhattacharya, D., and Falkowski, P.G. (2016). Temporal and spatial expression patterns of biomineralization proteins during early development in the stony coral *Pocillopora damicornis*. Proceedings of the Royal Society of London B: Biological Sciences *283*.
5. Moya, A., Huisman, L., Ball, E.E., Hayward, D.C., Grasso, L.C., Chua, C.M., Woo, H.N., Gattuso, J.P., Forêt, S., and Miller, D.J. (2012). Whole transcriptome analysis of the coral *Acropora millepora* reveals complex responses to CO_2-driven acidification during the initiation of calcification. Mol. Ecol. *21*, 2440–2454.
6. Puverel, S., Tambutte, E., Zoccola, D., Domart-Coulon, I., Bouchot, A., Lotto, S., Allemand, D., and Tambutte, S. (2005). Antibodies against the organic matrix in scleractinians: a new tool to study coral biomineralization. Coral Reefs *24*, 149–156.
7. Mass, T., Drake, J.L., Haramaty, L., Kim, J.D., Zelzion, E., Bhattacharya, D., and Falkowski, P.G. (2013). Cloning and characterization of four novel coral acid-rich proteins that precipitate carbonates *in vitro*. Curr. Biol. *23*, 1126–1131.
8. Drake, J.L., Mass, T., Haramaty, L., Zelzion, E., Bhattacharya, D., and Falkowski, P.G. (2013). Proteomic analysis of skeletal organic matrix from the stony coral *Stylophora pistillata*. Proc. Natl. Acad. Sci. USA *110*, 3788–3793.

9. Ramos-Silva, P., Kaandorp, J., Huisman, L., Marie, B., Zanella-Cléon, I., Guichard, N., Miller, D.J., and Marin, F. (2013). The skeletal proteome of the coral *Acropora millepora*: the evolution of calcification by co-option and domain shuffling. Mol. Biol. Evol. *30*, 2099–2112.
10. Takeuchi, T., Yamada, L., Shinzato, C., Sawada, H., and Satoh, N. (2016). Stepwise Evolution of Coral Biomineralization Revealed with Genome-Wide Proteomics and Transcriptomics. PLoS ONE *11*, e0156424.
11. Gal, A., Kahil, K., Vidavsky, N., DeVol, R.T., Gilbert, P.U.P.A., Fratzl, P., Weiner, S., and Addadi, L. (2014). Particle Accretion Mechanism Underlies Biological Crystal Growth from an Amorphous Precursor Phase. Adv. Funct. Mater. *24*, 5420–5426.
12. Falini, G., and Fermani, S. (2017). Nucleation and Growth from a Biomineralization Perspective. In New Perspectives on Mineral Nucleation and Growth: From Solution Precursors to Solid Materials, A.E.S. Van Driessche, M. Kellermeier, L.G. Benning, and D. Gebauer, eds. (Cham: Springer International Publishing), pp. 185–197.
13. Suzuki, M., Saruwatari, K., Kogure, T., Yamamoto, Y., Nishimura, T., Kato, T., and Nagasawa, H. (2009). An acidic matrix protein, Pif, is a key macromolecule for nacre formation. Science *325*, 1388–1390.
14. Addadi, L., and Weiner, S. (1985). Interactions between acidic proteins and crystals: stereochemical requirements in biomineralization. Proc. Natl. Acad. Sci. USA *82*, 4110–4114.
15. Von Euw, S., Zhang, Q., Manichev, V., Murali, N., Gross, J., Feldman, L.C., Gustafsson, T., Flach, C., Mendelsohn, R., and Falkowski, P.G. (2017). Biological control of aragonite formation in stony corals. Science *356*, 933–938.
16. Mass, T., Giuffre, A.J., Sun, C.-Y., Stifler, C.A., Frazier, M.J., Neder, M., Tamura, N., Stan, C.V., Marcus, M.A., and Gilbert, P.U.P.A. (2017). Amorphous calcium carbonate particles form coral skeletons. Proceedings of the National Academy of Sciences *114*, E7670–E7678.
17. Akiva, A., Malkinson, G., Masic, A., Kerschnitzki, M., Bennet, M., Fratzl, P., Addadi, L., Weiner, S., and Yaniv, K. (2015). On the pathway of mineral deposition in larval zebrafish caudal fin bone. Bone *75*, 192–200.
18. Kerschnitzki, M., Akiva, A., Ben Shoham, A., Asscher, Y., Wagermaier, W., Fratzl, P., Addadi, L., and Weiner, S. (2016). Bone mineralization pathways during the rapid growth of embryonic chicken long bones. J. Struct. Biol. *195*, 82–92.
19. Vidavsky, N., Addadi, S., Mahamid, J., Shimoni, E., Ben-Ezra, D., Shpigel, M., Weiner, S., and Addadi, L. (2014). Initial stages of calcium uptake and mineral deposition in sea urchin embryos. Proc. Natl. Acad. Sci. USA *111*, 39–44.
20. Khalifa, G.M., Kirchenbuechler, D., Koifman, N., Kleinerman, O., Talmon, Y., Elbaum, M., Addadi, L., Weiner, S., and Erez, J. (2016). Biomineralization pathways in a foraminifer revealed using a novel correlative cryo-fluorescence-SEM-EDS technique. J. Struct. Biol. *196*, 155–163.
21. Mass, T., Drake, J.L., Haramaty, L., Rosenthal, Y., Schofield, O.M.E., Sherrell, R.M., and Falkowski, P.G. (2012). Aragonite precipitation by "proto-polyps" in coral cell cultures. PLoS ONE *7*, e35049.
22. Helman, Y., Natale, F., Sherrell, R.M., Lavigne, M., Starovoytov, V., Gorbunov, M.Y., and Falkowski, P.G. (2008). Extracellular matrix production and calcium carbonate precipitation by coral cells in vitro. Proc. Natl. Acad. Sci. USA *105*, 54–58.
23. Drake, J.L., Schaller, M.F., Mass, T., Godfrey, L., Fu, A., Sherrell, R.M., Rosenthal, Y., and Falkowski, P.G. Molecular and geochemical perspectives on the influence of CO_2 on calcification in coral cell cultures. Limnol. Oceanogr., Published July 21, 2017. 10.1002/lno.10617.
24. Jokiel, P.L., Maragos, J.E., and Franzisket, L. (1978). Coral growth: buoyant weight technique. In Coral Reefs: Research Methods, D.R. Stoddart, and R.E. Johannes, eds. (UNESCO), pp. 529–541.
25. Ren, D., Albert, O., Sun, M., Müller, W.E.G., and Feng, Q. (2014). Primary cell culture of fresh water *Hyriopsis cumingii* mantle/pearl sac tissues and its effect on calcium carbonate mineralization. Cryst. Growth Des. *14*, 1149–1157.
26. Moya, A., Tambutté, S., Tambutté, E., Zoccola, D., Caminiti, N., and Allemand, D. (2006). Study of calcification during a daily cycle of the coral *Stylophora pistillata*: implications for 'light-enhanced calcification'. J. Exp. Biol. *209*, 3413–3419.
27. Zoccola, D., Tambutté, E., Kulhanek, E., Puverel, S., Scimeca, J.C., Allemand, D., and Tambutté, S. (2004). Molecular cloning and localization of a PMCA P-type calcium ATPase from the coral Stylophora pistillata. Biochim. Biophys. Acta *1663*, 117–126.
28. Bertucci, A., Moya, A., Tambutté, S., Allemand, D., Supuran, C.T., and Zoccola, D. (2013). Carbonic anhydrases in anthozoan corals-A review. Bioorg. Med. Chem. *21*, 1437–1450.
29. Vidavsky, N., Addadi, S., Schertel, A., Ben-Ezra, D., Shpigel, M., Addadi, L., and Weiner, S. (2016). Calcium transport into the cells of the sea urchin larva in relation to spicule formation. Proc. Natl. Acad. Sci. USA *113*, 12637–12642.
30. Ōmori, M., and Watabe, N. (1980). The mechanisms of biomineralization in animals and plants: Proceedings of the Third International Biomineralization Symposium (Tokai University Press).
31. Jackson, D.J., Thiel, V., and Wörheide, G. (2010). An evolutionary fast-track to biocalcification. Geobiology *8*, 191–196.
32. Le Tissier, M.D.A.A. (1988). Patterns of formation and the ultrastructure of the larval skeleton of Pocillopora damicornis. Marine Biology *98*, 493–501.
33. Johnston, I.S. (1980). The ultrastructure of skeletogenesis in hermatypic corals. Int. Rev. Cytology *67*, 171–214.
34. Clode, P.L., and Marshall, A.T. (2002). Low temperature FESEM of the calcifying interface of a scleractinian coral. Tissue Cell *34*, 187–198.
35. Tambutté, E., Allemand, D., Zoccola, D., Meibom, A., Lotto, S., Caminiti, N., and Tambutté, S. (2007). Observations of the tissue-skeleton interface in the scleractinian coral *Stylophora pistillata*. Coral Reefs *26*, 517–529.
36. Allemand, D., TambuttE, E., Girard, J.P., and Jaubert, J. (1998). Organic matrix synthesis in the scleractinian coral *stylophora pistillata*: role in biomineralization and potential target of the organotin tributyltin. J. Exp. Biol. *201*, 2001–2009.
37. Hamm, L.M., Giuffre, A.J., Han, N., Tao, J., Wang, D., De Yoreo, J.J., and Dove, P.M. (2014). Reconciling disparate views of template-directed nucleation through measurement of calcite nucleation kinetics and binding energies. Proc. Natl. Acad. Sci. USA *111*, 1304–1309.
38. Giuffre, A.J., Hamm, L.M., Han, N., De Yoreo, J.J., and Dove, P.M. (2013). Polysaccharide chemistry regulates kinetics of calcite nucleation through competition of interfacial energies. Proc. Natl. Acad. Sci. USA *110*, 9261–9266.
39. Addadi, L., Joester, D., Nudelman, F., and Weiner, S. (2006). Mollusk shell formation: a source of new concepts for understanding biomineralization processes. Chemistry *12*, 980–987.
40. Pan, C., Fang, D., Xu, G., Liang, J., Zhang, G., Wang, H., Xie, L., and Zhang, R. (2014). A novel acidic matrix protein, PfN44, stabilizes magnesium calcite to inhibit the crystallization of aragonite. J. Biol. Chem. *289*, 2776–2787.
41. Politi, Y., Mahamid, J., Goldberg, H., Weiner, S., and Addadi, L. (2007). Asprich mollusk shell protein: *in vitro* experiments aimed at elucidating function in $CaCO_3$ crystallization. CrystEngComm *9*, 1171–1177.
42. Meibom, A., Cuif, J.-P., Hillion, F., Constantz, B.R., Juillet-Leclerc, A., Dauphin, Y., Watanabe, T., and Dunbar, R.B. (2004). Distribution of magnesium in coral skeleton. Geophysical Research Letters *31*, L23306.
43. Zoccola, D., Moya, A., Béranger, G.E., Tambutté, E., Allemand, D., Carle, G.F., and Tambutté, S. (2009). Specific expression of BMP2/4 ortholog in biomineralizing tissues of corals and action on mouse BMP receptor. Mar. Biotechnol. (NY) *11*, 260–269.
44. Vancha, A.R., Govindaraju, S., Parsa, K.V.L., Jasti, M., González-García, M., and Ballestero, R.P. (2004). Use of polyethyleneimine polymer in cell culture as attachment factor and lipofection enhancer. BMC Biotechnol. *4*, 23.
45. Chen, B.-C., Legant, W.R., Wang, K., Shao, L., Milkie, D.E., Davidson, M.W., Janetopoulos, C., Wu, X.S., Hammer, J.A., 3rd, Liu, Z., et al.

(2014). Lattice light-sheet microscopy: imaging molecules to embryos at high spatiotemporal resolution. Science *346*, 1257998.

46. Gao, L., Shao, L., Chen, B.-C., and Betzig, E. (2014). 3D live fluorescence imaging of cellular dynamics using Bessel beam plane illumination microscopy. Nat. Protoc. *9*, 1083–1101.
47. Planchon, T.A., Gao, L., Milkie, D.E., Davidson, M.W., Galbraith, J.A., Galbraith, C.G., and Betzig, E. (2011). Rapid three-dimensional isotropic imaging of living cells using Bessel beam plane illumination. Nat. Methods *8*, 417–423.
48. Swanson, R., and Hoegh-Guldberg, O. (1998). Amino acid synthesis in the symbiotic sea anemone *Aiptasia pulchella*. Mar. Biol. *131*, 83–93.
49. Kopp, C., Pernice, M., Domart-Coulon, I., Djediat, C., Spangenberg, J.E., Alexander, D.T.L., Hignette, M., Meziane, T., and Meibom, A. (2013). Highly dynamic cellular-level response of symbiotic coral to a sudden increase in environmental nitrogen. MBio *4*, e00052–e13.
50. Roberts, J.M., Davies, P.S., Fixter, L.M., and Preston, T. (1999). Primary site and initial products of ammonium assimilation in the symbiotic sea anemone *Anemonia viridis*. Mar. Biol. *135*, 223–236.
51. Paulsson, M., Sommarin, Y., and Heinegård, D. (1983). Metabolism of cartilage proteins in cultured tissue sections. Biochem. J. *212*, 659–667.
52. Cserzö, M., Eisenhaber, F., Eisenhaber, B., and Simon, I. (2002). On filtering false positive transmembrane protein predictions. Protein Eng. *15*, 745–752.
53. Hofmann, K., and Stoffel, W. (1993). TMbase - A database of membrane spanning proteins segments. Biol. Chem. Hoppe Seyler *374*, 166.
54. Krogh, A., Larsson, B., von Heijne, G., and Sonnhammer, E.L. (2001). Predicting transmembrane protein topology with a hidden Markov model: application to complete genomes. J. Mol. Biol. *305*, 567–580.
55. Gabitov, R.I., Gagnon, A.C., Guan, Y., Eiler, J.M., and Adkins, J.F. (2013). Accurate Mg/Ca, Sr/Ca, and Ba/Ca ratio measurements in carbonates by SIMS and NanoSIMS and an assessment of heterogeneity in common calcium carbonate standards. Chem. Geol. *356*, 94–108.
56. John, S.G., and Adkins, J.F. (2010). Analysis of dissolved iron isotopes in seawater. Mar. Chem. *119*, 65–76.
57. Schindelin, J., Arganda-Carreras, I., Frise, E., Kaynig, V., Longair, M., Pietzsch, T., Preibisch, S., Rueden, C., Saalfeld, S., Schmid, B., et al. (2012). Fiji: an open-source platform for biological-image analysis. Nat. Methods *9*, 676–682.
58. Schneider, C.A., Rasband, W.S., and Eliceiri, K.W. (2012). NIH Image to ImageJ: 25 years of image analysis. Nat. Methods *9*, 671–675.

STAR★METHODS

KEY RESOURCES TABLE

REAGENT or RESOURCE	SOURCE	IDENTIFIER
Antibodies		
CARP1 primary antibody	Thermo Fisher Scientific Custom Antibody Services; [3]	custom
CARP4 primary antibody	Thermo Fisher Scientific Custom Antibody Services; [3]	custom
Alexa Fluor 405 goat-anti-rabbit secondary antibody	Life Technologies	Cat# A-31556; RRID: AB_221605
Biological Samples		
Stylophora pistillata nubbins	Rutgers University, Department of Marine and Coastal Sciences, in-house aquarium; [21]	fnatale@marine.rutgers.edu
Chemicals, Peptides, and Recombinant Proteins		
Dulbecco's Modified Eagle Medium	Sigma	Cat# D5030
Anti-biotics/mycotics Cocktail	GIBCO	Cat #15240062
Heat-inactivated fetal bovine serum	Invitrogen	Cat# 16140071
Poly(ethyleneimine) solution	Sigma	Cat# P3143
L-Aspartic Acid, 98+ atom%, ^{15}N	Sigma	Cat# 332135
Software and Algorithms		
ThresholdAnalysis.application	This paper	https://zenodo.org/record/840601
Unstacker.m	This paper	https://zenodo.org/record/840601
Other		
#1 5 mm round coverslips	Warner Instruments	64-0700 CS-5R
CARP1	N/A [7]	GenBank: KC148537.1
CARP4	N/A [8]	GenBank: KC493647.1

CONTACT FOR REAGENT AND RESOURCE SHARING

Further information and requests for resources and reagents should be directed to and will be fulfilled by the Lead Contact, Tali Mass (tmass@univ.haifa.ac.il).

EXPERIMENTAL MODEL AND SUBJECT DETAILS

Cell cultures of the Indo-Pacific stony coral *Stylophora pistillata* were prepared from nubbins contained in an in-house 800-L aquarium following methods of Mass et al. [21]. Nubbins were obtained from the Long Island Aquarium and Exhibition Center in 2011 from a single original parent colony, likely originally from Australia, and reared as sub-nubbins until the present experiments.

METHOD DETAILS

Cell culture preparation

Cellular adhesion was disrupted by incubating the cultures for 4 hours in calcium-free seawater plus 3% antibiotics/mycotics (GIBCO) and 20 μg/L chloramphenicol. During this time, growth medium was prepared as follows: Instant Ocean (company) was mixed with Dulbecco's Modified Eagle Medium (DMEM, Sigma D5030) plus additives to achieve the following: 12.5% DMEM (at 8.3 g/L containing 0.578 g/L L-glutamine, 0.05 g/L taurine), 20 μg/L aspartic acid, 50 μg/L ascorbic acid, 2% heat-inactivated fetal bovine serum (Invitrogen), 0.1 mM glucose, 25 mM HEPES, and 1% anti-biotics/mycotics cocktail (GIBCO); pH was adjusted to 8.2 with NaOH. During secondary incubations, cells and tissue were allowed to spontaneously dissociate from nubbin skeletons during 24-hour incubation in the growth medium. Dissociated cells and tissue were gently pipetted away from the skeleton and pelleted at ~5000 × g. Pellets were resuspended in fresh medium and filtered through a 20 μm mesh into Primaria dishes. All incubations and culturing were conducted at room temperature under ambient light:dark cycles. It has previously been shown that cell-free medium and cultures killed with 15 mM sodium azide neither re-aggregate into proto-polyps nor precipitate $CaCO_3$ [21].

Antibody staining

S. pistillata cells and proto-polyps were immuno-labeled and analyzed by confocal microscopy in two experiments. In the first experiment, cultures were grown in Primaria wells containing 1 cm glass slides on which cells settled and adhered. Cultures were terminated and fixed after 1 and 5 days of growth. In the second experiment, samples from the LLSM time-lapse (described below) were used. All samples were fixed with 2% glutaraldehyde in phosphate buffered saline (PBS) at pH 8 for 4 hr without agitation, followed by two rinses in Tris buffered saline with 0.05% Tween (TBS-T) and dehydration in an ethanol series. Following modified methods of Zocolla et al. [43], fixed samples on culture slides were blocked for 1 hr in 0.05% TBS-T, 0.2% gelatin, 5% bovine serum albumin (BSA), and rinsed 3 × 5 min and 1 × 15 min in 0.05% TBS-T. Samples were incubated for 45 minutes in primary antibodies against either CARP1 or CARP4 (both 1:500 in 0.05% TBS-T) [3] at 37°C followed by 4 × 5 minute rinses in 0.05% TBS-T. Secondary incubations were conducted in Alex Fluor 405 goat-anti-rabbit (Life Technologies; 1:200 in 0.05% TBS-T) for 30 min at 37°C with the chamber covered in aluminum foil, followed by 3 × 5 min rinses in 0.05% TBS-T in a dark room. Labeled samples were stored in TBS, pH 7.7, at 4°C and observed with a confocal laser scanning microscope (Zeiss LSM 710 and Zeiss LMS880). Controls were performed without primary antibodies.

Lattice light sheet microscopy (LLSM) sample preparation

For live imaging by lattice light-sheet microscopy, #1 5-mm round coverslips (Warner Instruments 64-0700 CS-5R) were pretreated overnight at room temperature with poly(ethyleneimine) solution (Sigma# P 3143) at 100 μg/ml in 12 mM borate buffer in deionized water (pH 8.5) [44]. The pretreated coverslips were then placed in cell culture Primaria dishes. The cultures were checked every day for settlement. After two days proto-polyps were detected and the coverslips were stabilized in a custom-made stainless-steel holder. Once in the holder the samples were incubated for 1h in culture media containing 20 μM calcein. The holder was then affixed to piezo stages (Physik Instrumente (http://aicblog.janelia.org/?p=160). Imaging was conducted at 25°C in growth media and 200 nM calcein [45]. In order to reduce bleaching of the fluorescence signal, the media in the bath were replaced every 4 hr during the 72 hr imaging period with fresh growth media containing 200 nM calcein. Images were acquired via 1.1 NA 25X water-dipping objective (Nikon) at 12 points of interest every 5 min, using 300 mW MPB laser (488 nm). Bessel-beam plane illumination microscopy has been previously published [46, 47]. The lattice pattern was dithered along the x axis and sample was moved through the light sheet (stationary in Z). Deconvolution and deskewing was performed using Richardson-Lucy iterations and movies were made using the NIS Elements (Nikon).

After the LLSM experiments, two-photon imaging was performed on the same sample, prior to immunolocalization with CARP1 antibody, with a Bergamo II multi-photon microscope (Thorlabs Imaging Systems), equipped with an 8 kHz resonant scanner for video-rate imaging. Excitation laser was Chameleon Vision 2 (Coherent) and the objective used was CFI75 APO LWD 25XW (Nikon).

^{15}N Labeling and Secondary Ion Mass Spectrometry (SIMS)

Unlabeled growth medium containing 1 cm glass slides was exchanged for 30 min with medium containing 20 μg/L ^{15}N-labeled aspartic acid (Aldrich) at 5, 9, and 12 days. This length of time was chosen as corals show minimum catabolism of aspartic acid within this window [36, 48–50] while still incorporating the amino acid into protein [36, 51]. After 30 min, labeled growth medium was discarded, and the proto-polyps were rinsed with unlabeled medium 3 × 3 min and allowed to grow in unlabeled medium until the next time point or for one hour until termination and fixation. After ^{15}N aspartic acid incubation, rinsing, and final unlabeled incubation, 12 day old samples on glass slides were fixed in 2% glutaraldehyde in PBS at pH 8.2 for 4 hr, then dehydrated in an ethanol series and stored in 100% ethanol at −20°C until critical point drying in CO_{2liq}. Dried slides were coated in 10 nm Au and imaged on a Phenom Pro X scanning electron microscope with energy dispersive spectroscopy (EDS). Calcium-containing particles on or adjacent to *S. pistillata* proto-polyps were confirmed by point-analysis with EDS at the Ca Kα peak at 3.6-3.8 keV, Mg Kα peak at 1.15-1.35 keV, and Na Kα peak at 0.91-1.13 keV.

S. pistillata proto-polyps were analyzed on a Cameca NanoSIMS 50-L after applying a 30 nm gold coating to increase conductivity. Select proto-polyp regions of interest (ROIs) were pre-sputtered with a positive primary beam (Cs^+; ~1 pA) for five minutes followed by 14 or 27.5 ms/pixel dwell times for sample analysis. Each ROI was analyzed for secondary ions of masses 25.924 ($^{14}N/^{12}C^-$), 27.002 ($^{15}N/^{12}C^-$), and 39.798 ($^{40}Ca^-$) amu with as many as seven layers collected per ROI and using the electron gun to reduce surface charging. Because the ionization efficiency of Ca to negative ions is low, the 39.798 amu mass peak was checked against a calcite standard. ROIs were 10 × 10 μm and analyzed as 265 × 265-point grids, resulting in ~40 nm pixel sizes. Each ROI was later re-imaged by SEM with EDS.

CARPs Transmembrane Prediction

Consensus transmembrane predictions for CARPs 1-4 (GenBank Accession numbers AGE35225.2, AGE35227.1, AGE36226.1, and AGG36357.1, respectively) were generated in TMpred, TMHMM, and DAS TM filter servers using server default settings [52–54].

QUANTIFICATION AND STATISTICAL ANALYSIS

Antibody Staining

Cell cultures were grown in duplicate wells with up to three slides per well (one each for CARP1 and CARP4 antibodies and controls), with duplicate individual wells for each sampling time-point. A minimum of five regions of interest (ROIs) on each slide were examined by confocal microscopy or LLSM.

LLSM Calcein Imaging

Calcein incorporation into ECM was imaged at 12 locations within a calcein-labeled cell culture. Ten ROIs were examined from a separate cell culture labeled with calcein to track single crystal growth.

^{15}N Labeling and Secondary Ion Mass Spectrometry (SIMS)

Cell cultures were grown in wells with two slides per well, with duplicate individual wells for each sampling time-point. At least five ROIs per slide were examined by SEM with EDS. Five ROIs from a single slide of 12 d proto-polyps were then analyzed by NanoSIMS. NanoSIMS pixel counts for masses $^{14}N/^{12}C^-$, $^{15}N/^{12}C^-$, and $^{40}Ca^-$ averaged ~900, 7, and 6 total counts per pixel, respectively. We used the natural abundance of $^{15}N/^{14}N$, 0.0036, as a cutoff for the measured $^{15}N/^{12}C^-$:$^{14}N/^{12}C^-$ values and only plot points that exceed the cutoff in Figure 4A. The NanoSIMS has been shown to be a Poisson statistics machine for a wide range of elemental and isotopic ratios and for a wide range of total counts [55]. To check the robustness of enriched points over and above the natural abundance background we propagated errors based on the "effective" number of counts for the $^{15}N/^{12}C^-$:$^{14}N/^{12}C^-$ ratio [56] and found 85% of the points exceeded the 1 s bound, even for these small signal sizes. Images of isotope and element ratios using these cutoffs were generated using the OpenMIMS open-source plug-in for FIJI image processing software [57, 58].

DATA AND SOFTWARE AVAILABILITY

LLSM Single Crystal Growth Rate

In order to calculate single aragonite crystal growth rate, images were first de-stacked using a MATLAB code and a Threshold Analysis app was created. This app enables the visualization of the un-stacked data, and by using simple photo editing tools to crop and enhancing point of interest. The data then are exported to spreadsheets to simplify numeric data analysis. Code is available at https://zenodo.org/record/840601.